Journal of Alloys and Compounds 480 (2009) 422–427

Contents lists available at ScienceDirect

Journal of Alloys and Compounds

journal homepage: www.elsevier.com/locate/jallcom

Review

Effect of heat treatment on the microstructure and mechanical properties of Fe-based amorphous coatings

Fu Bin-you [a,b,*], He Ding-yong [a], Zhao Li-dong [b]

[a] College of Materials Science and Engineering, Beijing University of Technology, Beijing 100124, China
[b] Surface Engineering Institute, RWTH Aachen University, Juelicher Str. 334a, Germany

ARTICLE INFO

Article history:
Received 26 June 2008
Received in revised form 22 February 2009
Accepted 24 February 2009
Available online 9 March 2009

Keywords:
Amorphous
Heat treatment
Microstructure
Mechanical properties

ABSTRACT

Amorphous coatings were fabricated by arc spraying and the effect of the post heat treatment on the microstructure, and the mechanical properties of arc sprayed coatings were studied. Post heat treatment was conducted in the atmospheric environment within the temperature ranged from 500 °C to 800 °C. The microstructure characteristics were analyzed by means of optical microscopy (OM), X-ray diffraction (XRD), electron probe micro-analyzer (EPMA), scanning electron microscopy (SEM), differential thermal analysis (DTA) and transmission electron microscopy (TEM). It was found that with the increase of anneal temperature, the microstructure of the sprayed coatings had several changes as follows: the reduction of porosity, the decomposition and the crystallization of amorphous phase, and the formation of precipitates. The microhardness of the sprayed coatings increased after the heat treatment and it can reached to 1275 HV_{300g} at the post treated at 600 °C. All the coatings exhibited an excellent abrasive wear resistance, approximately 6 times higher than that of the arc-sprayed 3Cr13 coating.

Contents

1. Introduction

Amorphous alloys have been of interest not only for fundamental studies, but also for potential applications for over 30 years. The advantages of the amorphous alloy such as high hardness, high corrosion and excellent wear resistance make them as a good candidate for many applications [1–4]. In recent years, several fabrication routes are under development to produce amorphous or amorphous/nanostructured materials. Among them, thermal spraying process is one of the amorphous forming technologies due to the sufficient rapid cooling rate that inhibits long-range diffusion and also avoids crystallization [5–9]. Compared with other thermal spray technologies, arc spraying is a unique spraying process with regard to the much lower costs and higher quality coatings [10–13].

Post heat treatment can be used to further improve the properties of sprayed coatings, such as laser remelting, shot peening, sealing and furnace heat treatment [14–16]. Lan et al. have found that the microstructure and characterization of the coatings were significantly affected by a post heat treatment, in which numerous metallurgy bonding was found in the interfaces between coatings and substrates. As a result, the thermal fatigue behavior of the sintered coatings was greatly improved [17]. The heat treatment of amorphous coatings leads to the precipitation of sub-micrometric crystals [18], which definitely enhances the mechanical properties of coatings, such as the microhardness, fracture toughness and wear resistance [19–22]. Yoo et al. [23] have found that the amorphous structured coatings exhibit a superior corrosion resistance to the crystallized coatings with high polarization resistance, and the

* Corresponding author at: College of Materials Science and Engineering, Beijing University of Technology, Beijing 100124, China. Tel.: +86 10 67392168; fax: +86 10 67392168.
E-mail address: binyou@emails.bjut.edu.cn (B.-y. Fu).

0925-8388/$ – see front matter © 2009 Published by Elsevier B.V.
doi:10.1016/j.jallcom.2009.02.107

corrosion resistance decreased after heat treatment. Studies on the post heat treatment of arc sprayed Fe-based amorphous coatings have not been reported so far, to the authors' knowledge.

The present study aimed at investigating the effect of post heat treatment on the microstructure and mechanical properties of arc sprayed Fe-based amorphous coatings.

2. Experimental

Cored wire in a diameter of 2.0 mm was used to produce amorphous coatings. The chemical composition of cored wire was (wt.%): 52.16 Fe, 36.18 Cr, 5.64 B, 5.64 Ni, 0.35 Si, and 0.03 C. The coatings were sprayed onto degreased and grit blasted Q235 steel substrates (56 mm × 25 mm × 5 mm) by arc spraying system (JZY-250, Beijing Jiazhiyuan Scientific & Trading Co., Ltd, China) under the optimized spray parameters. The parameters were as follows: arc voltage, 32 V; arc current, 180 A; air pressure, 0.55 MPa; spray distance, 100 mm. The samples were coated until the thickness being about 1000 μm. During spraying, the samples were not cooled by compressed air. After arc spraying, the coatings were annealed in a furnace in air at 500 °C, 600 °C, 700 °C and 800 °C for 1 h, and then cooled in air.

The microstructures of the coatings were investigated by means of optical microscopy (OM) and transmission electron microscopy (TEM). The transmission electron microscopy field images and selected area diffraction (SAD) patterns were obtained using JEM-2000FX TEM analytical electron microscope. The phases of the coatings were characterized by the X-ray diffraction (XRD) (D8 ADVANCE, BRUKER/AKS, Germany) using Cu Kα target at 40 kV and 20 mA. Composition analysis were performed in a JEOL JXA-8100 electron probe micro-analyzer (EPMA) operated at 20 kV, using a thin-window detector capable of analyzing elements with atomic number down to boron. Differential thermal analysis (DTA) was conducted using the STA-449C unit with the heating and cooling rate of 20 K/min in argon. The surfaces of the annealed coatings were polished to remove the formed oxide scales prior to being analyzed. The porosity of the coatings was evaluated through image analyzing of cross-sectional microstructure of the coatings. A total of 10 pictures of each coating were taken by an optical microscope at a magnification of 200 to evaluate the average porosity levels.

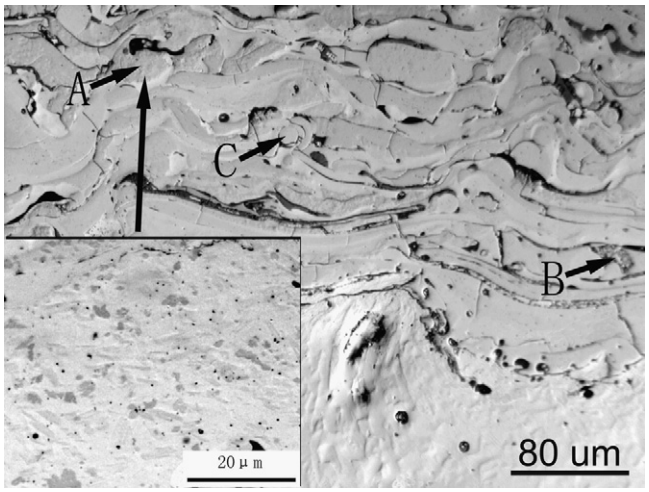

Fig. 1. Cross-sectional microstructure of the as-sprayed coating.

The microhardness of the coatings (Vickers scale) was measured using a microVickers hardness tester (MicroMet 1, Buehler). The measurements were carried out on the cross-sections of the coatings. A load of 100 g was selected for the values of the single lamella. A load of 300 g was selected for the average values of the coatings. The given microhardness value was the average of 10 measurements.

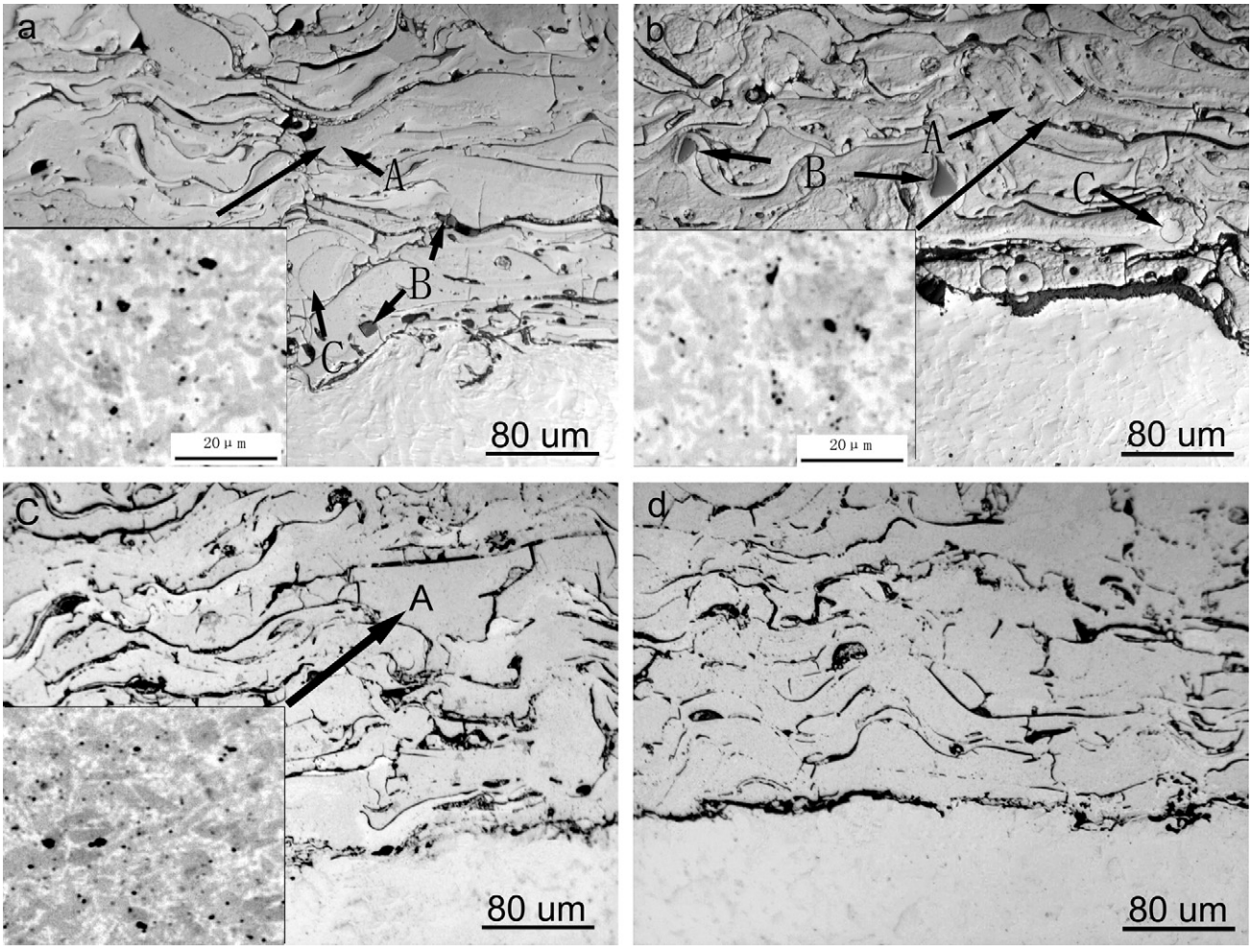

Fig. 2. Cross-sectional microstructure of the annealed coatings: (a) 500 °C annealing; (b) 600 °C annealing; (c) 700 °C annealing; (d) 800 °C annealing.

Table 1
The composition of different points in the as-sprayed coating (wt.%).

Points	Fe	Ni	Cr	B	C	Si
A	68.96	4.43	21.56	5.02	0.03	–
B	45.59	1.55	43.20	9.66	–	–
C	50.13	7.70	36.18	5.64	–	0.35

The abrasive wear test was carried out using a modified wet sand rubber wheel (Model MLS-225, Zhangjiakou Chengxin Balance Testing Machineries Company, China). The specimens' dimension was 57 mm × 25 mm × 6 mm and the coatings' thickness was 1.0 mm. The silicas in a sharp, angular morphology were used as abrasives and were sieved into the particle size range of 224–355 μm prior to the test. A load of 100 N was applied on the contact surface between the coating and the rubber wheel and the rubber wheel peripheral speed was 240 rpm. The specimen was immersed in the abrasive mortar with the weight ratio of $W_{silica}:W_{water}=3:2$. The tests were performed for a set number revolutions with a pre-abrading of 1000 cycles, and a refining abrading of 2000 cycles. The specimens were cleaned ultrasonically in the acetone bath for 3–5 min before and after the experiment. The weight loss of the specimen before and after abrasion was measured by a 0.1 mg BS224S electronic balance. An arc-sprayed 3Cr13 coating was also deposited for comparison. After the abrasive wear test, a square specimen of 5 mm × 5 mm was cut from the central part of the abrasive track. The wear track was examined by scanning electron microscopy (SEM).

3. Results and discussion

Fig. 1 shows the cross-sectional microstructure of the as-sprayed coatings. The coating consists of numerous flattened lamellae parallel to the substrate, indicating that most of sprayed droplets were in molten or semi-molten state as they impacted on the substrate. The microstructure of the as-sprayed coating is composed of three phases: the light metal lamellae (point A), the gray lamellae (point B) and unmelted particles (point C). The results of EPMA (as shown in Table 1) indicated that the light metal lamellae (point A) is Fe-rich phase and the higher magnification image showed that these lamellae contained small gray particles. It is presumed that borides evenly distribute in the metal matrix in these lamellae. The distributions of borides were not homogeneous in the coatings, for that some splats consist of lots of hard particles and some splats are comprised of few or none hard particles. The gray lamellae (point B) in as-sprayed coating could be the remained borides. The microhardness measurements showed that these gray lamellae were extremely hard, with the microhardness over 2600 HV_{100g}. These borides were not completely dissolved in molten Fe-matrix during spraying or the primarily crystallized borides in droplets with high B and Cr contents. Additionally, the unmelted particles in the coatings were occasionally identified by their near spherical morphology (point C). Some splat-boundary oxide stringers were also recognized as dark stringers in the optical micrographs.

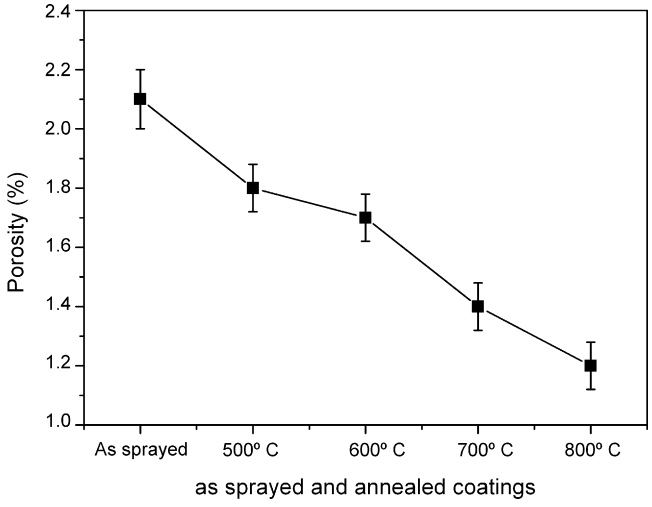

Fig. 3. Porosity of the as-sprayed and the annealed coatings.

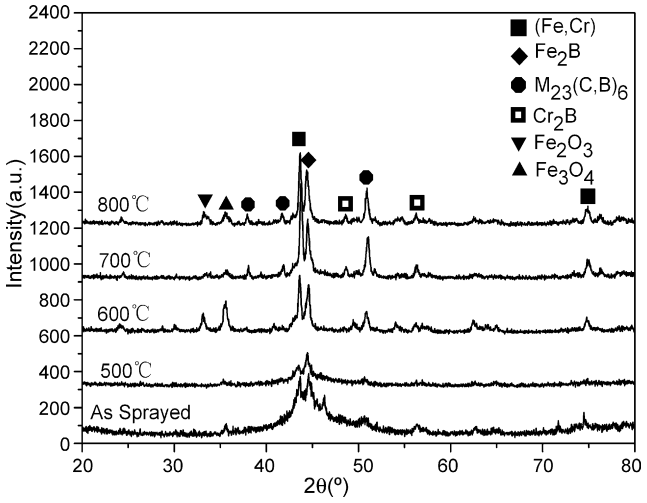

Fig. 4. XRD spectrum of the as-sprayed and the annealed coatings.

After annealing at 500 °C (Fig. 2a) and 600 °C (Fig. 2b), the morphology of the coating has not significant change. However, it is observed that there are more small dark precipitates in the light metal lamellae (the higher magnification images of the light metal

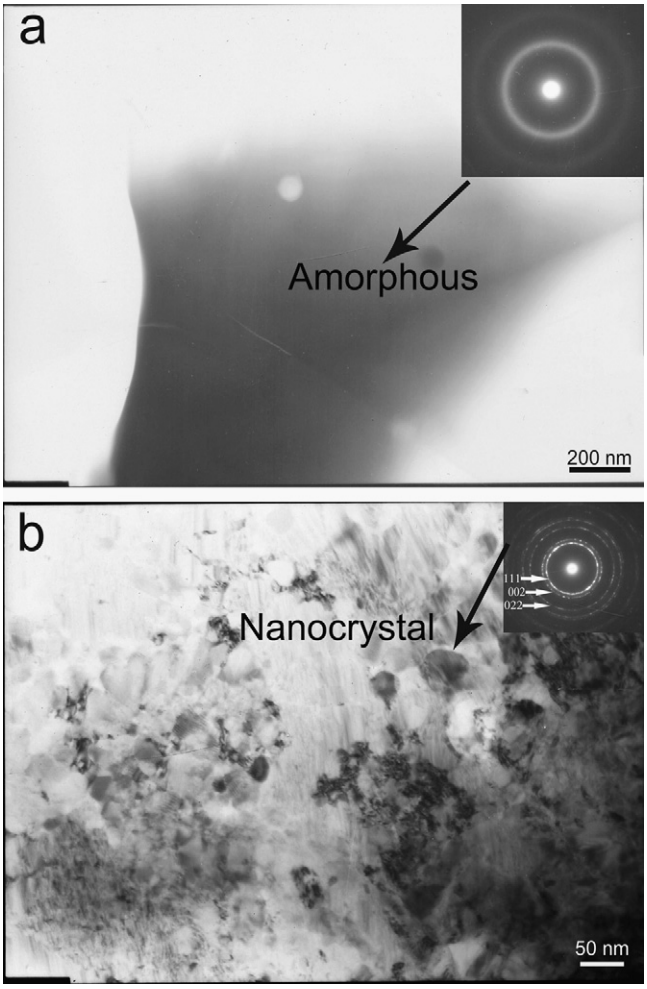

Fig. 5. TEM morphology of the as-sprayed and the annealed coating: (a) as-sprayed coating; (b) 600 °C annealing.

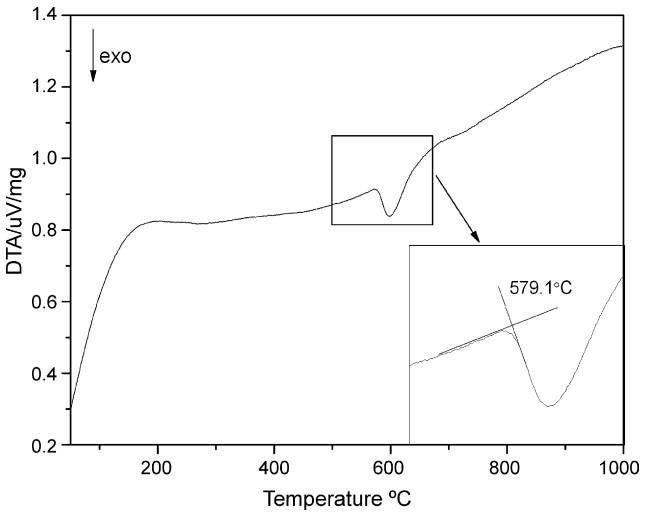

Fig. 6. DTA spectrum of the as-sprayed coating.

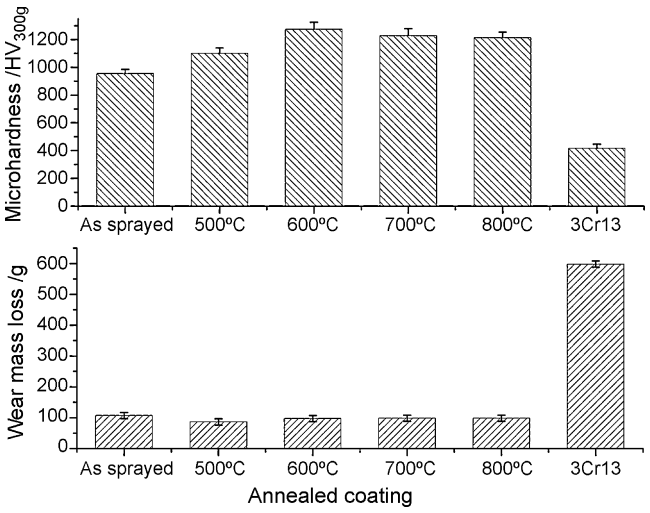

Fig. 7. Wear mass loss and microhardness of the as-sprayed and annealed coatings.

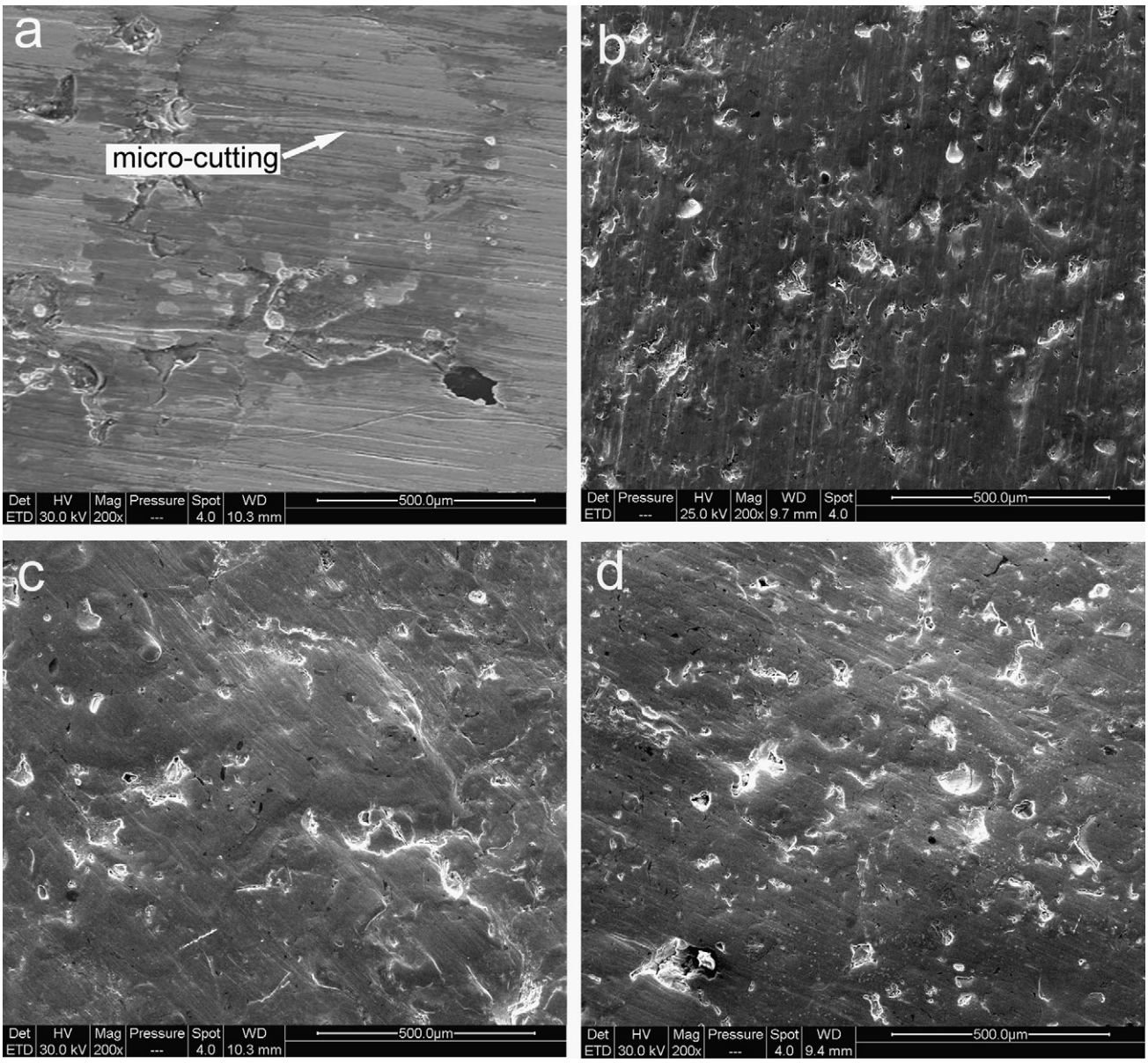

Fig. 8. Morphology of as-sprayed and annealed coatings after abrasive wear: (a) 3Cr13 coating; (b) as-sprayed coating; (c) 500 °C annealing; (d) 600 °C annealing.

lamellae are showed in bottom left corner of Fig. 2a and b), After annealing at 700 °C (Fig. 2c) and 800 °C (Fig. 2d), the modification of the coating's morphology is visible. Some original boundaries between thin lamellae get unclear, indicating that diffusion and sintering processes occurred during the heat treatment. Fig. 3 shows the porosity of as-sprayed and the annealed coatings. The as-sprayed coating has the highest porosity of about 2.1%, and small oxide stringers can be identified. After annealed, the porosity in the coatings has decreased to about 1–1.2%. The porosity decreased with the anneal temperature increasing. The structure of the coatings was densified as the sintering continued.

Fig. 4 demonstrates the XRD patterns of the as-sprayed and the annealed coatings. As shown in Fig. 4, a large hump at the X-ray diffraction angles of about 45° can be observed in the as-sprayed coating, indicating the amorphous phase was formed in the coating. In addition, the peaks in the diffraction patterns indicate that crystalline phases also exist in the as-sprayed coating. From the patterns, as-sprayed coating was mainly composed of Fe–Cr alloy and Fe_2B hard phase with a fraction of $M_{23}(C,B)_6$ and Fe_3O_4. The XRD analysis of the coating heat-treated at 500 °C reveals a very interesting result. As shown in Fig. 4, the intensities of all the phases identified in the coating heat-treated at 500 °C are much lower than those in the as-sprayed coating. However, it is very difficult to explain this phenomenon. After the heat treatment at 600 °C, the large hump pattern nearly disappears and the peaks become sharper and shift to the angle increasing direction (decreasing d-spacing). This is due to the crystallization of the amorphous phases. Another significant change in the XRD spectrum after the heat treatment at 600 °C is that Fe_2O_3 could be identified in the coating. After heat-treated at 700 °C and 800 °C, it can be seen that the intensities of the hard phases and the Fe-based phase coating increase further significantly. According to Scherrer formula, the measured grain size decreases as the FWHM (full-width half-maximum) increases; the calculate result shows that the average grain sizes of the as-sprayed, 500 °C, 600 °C, 700 °C, 800 °C were about 4 nm, 11 nm, 22 nm, 22 nm and 24 nm, respectively.

Transmission electron microscopy (TEM) was made to give more detailed information. In the as-sprayed coating, as revealed by the TEM image, the inset diffraction pattern was taken from the amorphous regions and showed the expected diffuse halo (showed in top left corner of Fig. 5a). In the coating heat-treated at 600 °C, it was found that the matrix of the coating comprised of nanocrystalline grains having grain size ranged between 20 nm and 50 nm, in accordance with the calculation results of the Scherrer formula. The nanocrystalline were identified as fcc Fe-based phase by polycrystalline selected-area-diffraction (SAD) ring pattern showed in top right corner of Fig. 5b. Differential thermal analysis (DTA) was conducted in order to confirm the decomposition of the amorphous phase. As shown in Fig. 6, at the temperature 579.1 °C, an exothermic reaction occurs, confirming the crystallization of the amorphous phase.

Fig. 7 shows the effect of heat treatment on the wear mass loss and microhardness (excluded the hard phase such as borides) of the coatings. As shown in Fig. 7, all the coatings are harder than the arc-sprayed 3Cr13 coating. For the amorphous coatings, the heat treatment at 500 °C leads to an increase of microhardness from 960 HV_{300g} to 1100 HV_{300g}. It is assumable that the increase in the microhardness is mainly caused by the precipitates which formed in sintered lamellae. The heat treatment at 600 °C leads to a higher increment of microhardness from 1100 HV_{300g} to 1275 HV_{300g}. This increment could be mainly attributed to the decomposition of the amorphous phase into nanocrystalline phase. Compared to the coating heat-treated at 600 °C, the heat treatment at 700 °C and 800 °C lead to a decrease in the microhardness. As mentioned above, sintering process has already been observed. It is assumable that the decrease of the microhardness could be attributed to the phenomenon of the grain growth which coarsened precipitations of the stable phases.

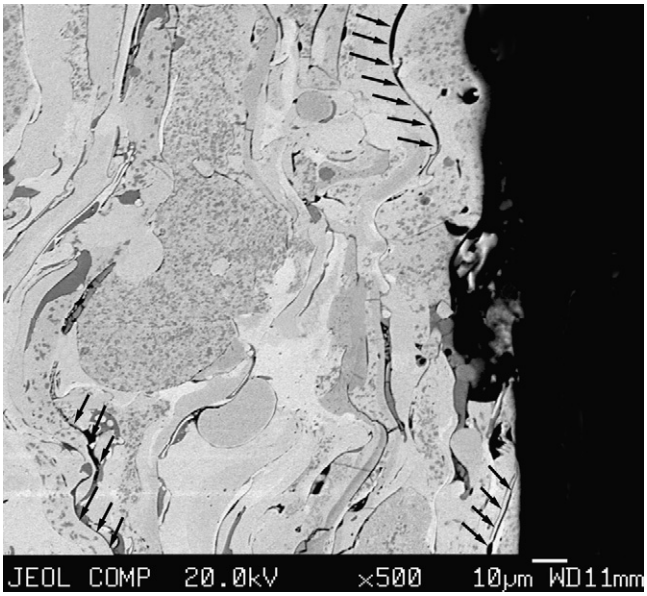

Fig. 9. Cross-sectional microstructure of the as-sprayed coating after abrasive wear.

The wear mass loss of the test samples are also showed in Fig. 7. Compared with the comparative sample (arc-sprayed 3Cr13 coating), all the coatings showed higher wear resistance. But the effect of heat treatment on the coatings's wear resistance is not obvious. The coating heat-treated at 500 °C shows the highest wear resistance, however the coatings heat-treated at 600 °C, 700 °C and 800 °C show the very similar results. Fig. 8 shows the morphology of the worn surfaces of the as-sprayed and that of the annealed coatings, and the arc-sprayed 3Cr13 coating as well. As shown in Fig. 8a, there are numerous plastic furrows on the worn surface of the 3Cr13 coating. It is believed that a typical micro-cutting mechanism makes sense. For the as-sprayed and the annealed coatings, only few slight plastic furrows can be seen on the worn surfaces. The high hardness strongly restrained the micro-cutting process. It is suggested that the primary mechanism of wear was by selective removal of the binder probably caused by the plastic deformation and fatigue due to the repeated action of the abrasive particles followed by the undermining of the borides particles resulting in their eventual pullout. Another mechanism is flaking off caused by micro-cracks. As shown in Fig. 9, there are lots of sub-surface micro-cracks on the cross-section of the as-sprayed amorphous coating (arrowed in Fig. 9). Under the abrasion conditions, micro-cracks could be formed and grown at the boundary between the oxides and the metallic lamellae. When the length of micro-cracks is larger than the critical size of crack, flaking off of the lamellae occurs.

4. Conclusions

In the present study, effect of heat treatment on the microstructure and the mechanical properties of arc sprayed amorphous coatings were investigated. The obtained results are summarized as follows:

1. As-sprayed coating shows a typical lamellar structure. Amorphous phase, crystallined phases (Fe,Cr), Fe_2B, Cr_2B, $M_{23}(C,B)_6$ and oxide could be identified in the coating.
2. The decomposition and crystallization of amorphous phase occurred at 579.1 °C. As the annealing temperature increases, the coating shows a reduction in porosity and a significant increase

in the coating hardness. The highest value of 1275 HV_{300g} could be obtained in the coating heat-treated at 600 °C.

3. All the coatings exhibit an excellent abrasive wear resistance, about 6 times higher than that of arc-sprayed 3Cr13 coating.

Acknowledgment

The authors gratefully acknowledge the financial support from the German Science Foundation (DFG) within the scope of the project ZH205/1-1 for carrying the part of above reported results.

References

[1] A. Inoue, B.L. Shen, C.T. Chang, Acta Mater. 52 (2004) 4093.
[2] S.J. Pang, T. Zhang, K. Asami, A. Inoue, Acta Mater. 50 (2002) 489.
[3] H.Z. Fang, X.D. Hui, G.L. Chen, J. Alloys Compd. 464 (2008) 292.
[4] H.S. Ni, X.H. Liu, X.C. Chang, W.L. Hou, W. Liu, J.Q. Wang, J. Alloys Compd. 467 (2009) 163.
[5] Y. Li, K.A. Khor, Surf. Coat. Technol. 150 (2002) 125.
[6] A. Kobayashi, S. Yano, H. Kimur, A. Inoue, Mater. Sci. Eng. B 148 (2008) 110.
[7] A.H. Dent, A.J. Horlock, D.G. McCartney, S.J. Harris, Surf. Coat. Technol. 139 (2001) 244.
[8] H. Choi, S. Yoon, G. Kim, H. Jo, C. Lee, Scripta Mater. 53 (2005) 125.
[9] S. Kumar, J. Kim, H. Kim, C. Lee, J. Alloys Compd. (2008), doi:10.1016/j.jallcom.2008.07.064.
[10] P. Rohan, S. Bouaricha, J.G. Legoux, P. Ctibor, S. Nourouzi, A. Vardelle, Proc. ITSC 2004; CD-Rom.
[11] J.J. Fang, Z.X. Li, Y.W. Shi, Appl. Surf. Sci. 254 (13) (2008) 3849.
[12] S.S. Madaeni, M.E. Aalami-Aleagha, P. Daraei, J. Membr. Sci. 320 (2008) 541.
[13] D.Y. He, B.Y. Fu, J.M. Jiang, X.Y. Li, J. Therm. Spray Technol. 17 (5–6) (2008) 757.
[14] C.H. Lee, K.O. Min, Surf. Coat. Technol. 132 (2000) 49.
[15] J. Gutiérrez, J.M. Barandiarán, P. Mínguez, Z. Kaczkowski, P. Ruuskanen, G. Vlasák, P. Svecd, P. Duhaj, Sens. Actuators A 106 (2003) 69.
[16] Y.R. Zhang, R.V. Ramanujan, Mater. Sci. Eng. A 416 (2006) 161.
[17] D.Y. Lan, Q. Wang, Z.Z. Xuan, Mater. Sci. Eng. A 473 (2008) 312.
[18] C. Garcıa, A. Zhukov, J. Gonzalez, V. Zhukova, R. Vargad, J.J. del Val, V. Larin, J.M. Blanco, J. Alloys Compd. 423 (2006) 116.
[19] S.Y. Park, M.C. Kim, C.G. Park, Mater. Sci. Eng. A 449–451 (2007) 894.
[20] G. Bolelli, L. Lusvarghi, J. Therm. Spray Technol. 15 (2006) 802.
[21] G. Bolelli, V. Cannillo, L. Lusvarghi, M. Montorsi, F.P. Mantini, M. Barletta, J. Wear 263 (2007) 1397.
[22] S.L. Wang, L.L. Hong, J. Alloys Compd. 429 (2007) 99.
[23] Y.H. Yoo, S.H. Lee, J.G. Kim, J.S. Kim, C. Lee, J. Alloys Compd. 461 (2008) 304.